Chapter 2 Experimental details

2-1 Techniques for the study

2-1-1 Auger Electron Spectroscopy (*AES*)

Auger electron spectroscopy is a standard technique in surface and interface physics. Its sensitivity is about 1% of a monolayer, thus, it is very suitable for studying the chemical composition of solid surfaces. Auger process is a secondary electron excitation process which is schematic as follows.

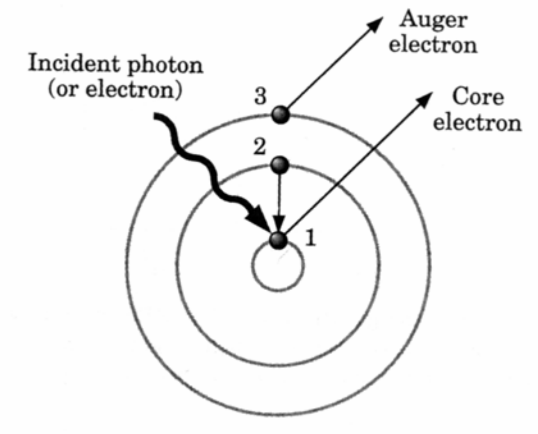

Fig. 2-1 The Auger process: a core electron (1) is ejected by an incident photon or electron; a second electron (2) falls into the resultant core holes; the energy lost by electron (2) can eject a third electron (3).

When an energetic beam of electrons (typically 3 keV in UHV) strikes the atom of a material, electrons which have binding energies less than the incident beam energy may be ejected from the inner atomic level. An excited atom is created by this ionized process. The electron vacancy thus is filled by deexcitation of electrons from other electron energy states. The energy released in the resulting electronic transition can be transferred by electrostatic interaction to still another electron in the same atom or in a different atom. Ultimately, it will be ejected into vacuum if this electron has a binding energy that is less than the energy transferred to it from filling the deep-lying electron vacancy. The electron ejected as a result of the deexcitation process is called an Auger electron.

For example, the primary hole is produced in the *K* shell, the Auger process is initiated by an outer electron from the *L* shell, e.g. the L_1 level as in Fig. 2-2. This electron falls into the initial *K* vacancy giving up its transition energy to another electron from the *L* shell, e.g. the L_3 shell; such an Auger process is termed a KL_1L_3 process. The KL_1L_3 process thus yields an Auger electron with the energy

$$E_{KL_1L_3} = E_K - E_{L_1} - E_{L_3}$$

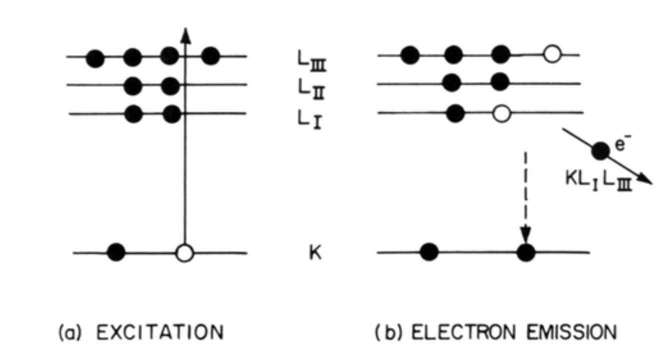

Fig. 2-2 Scheme of the Auger electron emission process.

In our studies, choosing the proper Auger transition is a very important step in the initial experiment. First, we must get all information of the corresponding transitions for the clean surface and the adsorbate-induced surface. The first derivative $dN(E)/dE$ of Auger spectra can be obtained as in Fig. 2-3.

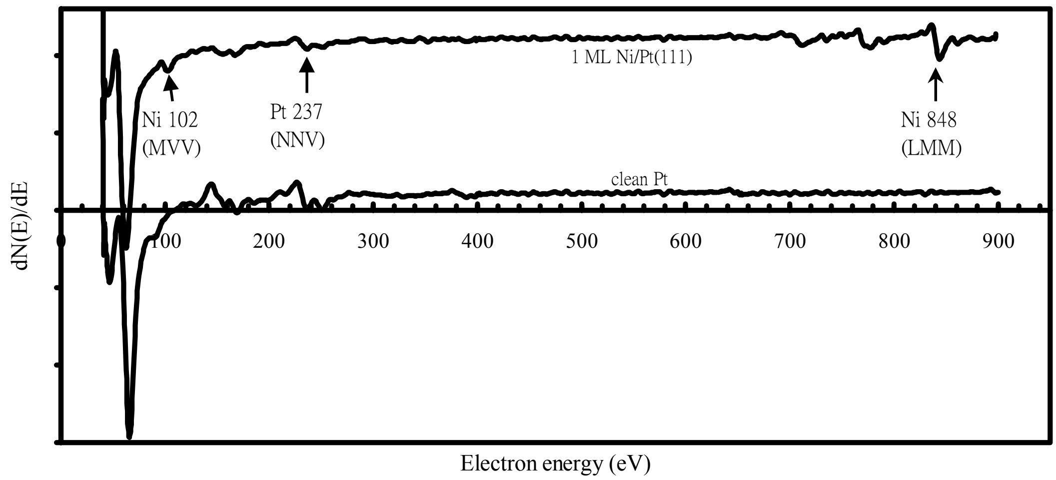

Fig. 2-3 The first derivative $dN(E)/dE$ of Auger spectra for clean Pt(111) surface and 1 monolayer (ML) of Ni grown on Pt(111) substrate were shown in the figure.

From the X-ray atomic energy level for specific element,[11] we can calculate the corresponding Auger transition of the distinct energy of the elements. For instance, the energy of $M_{2,3}$ level for Ni is 68.1 eV and the valence electron energy is 3.6 eV. Thus, the Auger transition of $M_{2,3}VV$ (V: valence e^- level)with an Auger electron energy $E_{M_{2,3}VV} = \ E_{M_{2,3}} - E_V - E_V = 60.9$ eV is possible. The Auger electron energy and its corresponding transition in this paper are collected and recalculated in the following table 2-1.

TABLE 2-1

Chemical element	Auger electron E(eV)	Assignment Transition	
Pt	237	$N_5N_6O_{4,5}$	(NNV)
Pt	64	$N_7O_{4,5}O_{4,5}$	(NVV)
Ag	351	$M_{4,5}N_{4,5}N_{4,5}$	(MVV)
Co	775	$L_3M_{4,5}M_{4,5}$	(LMM)
Co	53	$M_{2,3}M_{4,5}M_{4,5}$	(MVV)
Ni	848	$L_3M_{4,5}M_{4,5}$	(LMM)
Ni	102	$M_1M_{4,5}M_{4,5}$	(MVV)
Ni	61	$M_{2,3}M_{4,5}M_{4,5}$	(MVV)

2-1-2 Low-Energy Electron Diffraction (*LEED*)

LEED is the standard technique and is the availability of a straightforward line of analysis to probe structural information about the surface. The experimental set up of LEED consists of an electron gun to produce an electron beam with primary energies in the range of 20~500 eV and a display system for measuring the Bragg diffraction peak intensity (00 beam intensity).

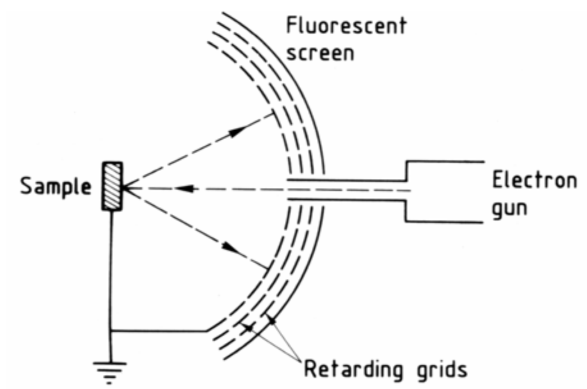

Fig. 2-4 Schematic LEED apparatus

In general, three types of information can be obtained from a LEED experiment:

1. The spot pattern indicates crystalline order and in epitaxial growth, and its symmetry from the sample surface. However, only the 2-dimentional

translational symmetry in the film plane can be deduced from visual inspection.

2. Taken LEED spot intensities I(E) measurement as a function of electron wavelength or energy E, one can get the information of third dimension along the surface normal. On the other hand, in combination with their analysis along the well-developed multiple-scattering theory,[12,13] I(E) analysis gives reliable data on relaxations.
3. For real structure and defect analysis, that which comes from a small angle analysis of the spot structure, performed in SPA-LEED. Because each surface atom can be considered as the source of a secondary wavelet, which actually sums up all multiple scattering processes ending up in this surface atom or atoms in a column below it, before the final emission. Due to the strong forward scattering of the electron and the small elastic mean free path involved, this wavelet depends only on a very narrow column around this surface atom. Moreover, the interference pattern of all wavelets can be treated by classical optical methods.

However, the energy range below 300 eV in particularly suited to surface studies since the mean-free path of these slow electrons in the solid is short enough to give good surface sensitivity. Furthermore, according to the de Broglie relation

$$\lambda\,(\text{Å}) = \frac{h}{p} = \sqrt{\frac{150.4}{E(eV)}} \tag{2-1}$$

Typically, LEED wavelengths are in the Ångstrom range and just the same order magnitude as the interatomic distances in a solid. When we used the common Bragg diffraction condition $2d\sin\theta = n\lambda$; where θ is the angle with respect to the surface plane; V_0 is the inner potential in the solid. One can obtain the mean interlayer spacing by the slope L_E in the Electron kinetic energy E versus n^2 relation:

$$d_i\,(\text{Å}) = \frac{1}{\sin\theta}\sqrt{\frac{150.4n^2}{4(E+V_0)}} = \frac{1}{\sin\theta}\sqrt{\frac{150.4}{4L_E}} \tag{2-2}$$

Here, the energy positions of the I(E) LEED for a clean Pt(111) is shown in the following Fig. 2-5. In our experimental setup the θ is typically perpendicular to surface normal (> 86°). Ultimately, we obtain the mean interlayer spacing of Pt(111) is 2.26 ± 0.01 Å.

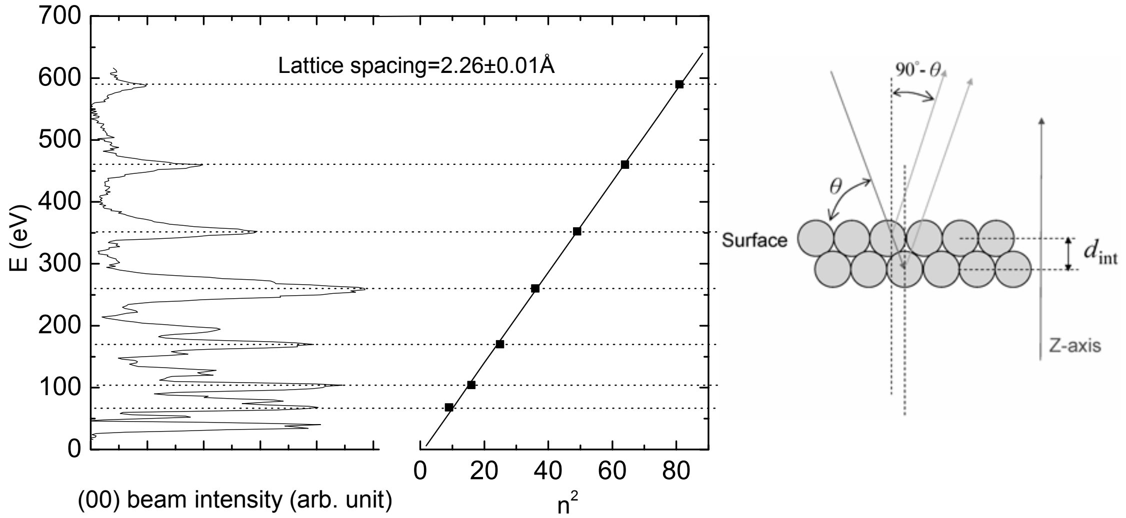

Fig. 2-5 Energy position of the I(E) peak sequences versus the index n^2 for clean Pt(111) surface at 300 K. The mean lattice spacing d_i = 2.26±0.01 Å was deduced from the slope of the straight line applying the following simple formula Eq. 2-2.

2-1-3 Ultraviolet Photoelectron Spectroscopy (*UPS*)

Experiments of this type yield the surface electron density of states, which has been found to be narrower than for the bulk. Because the bonding environment for surface atoms is very different in their number of nearest neighbors, e.g. relaxation or

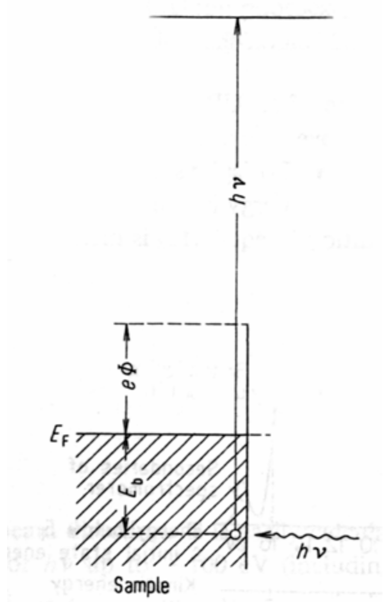

Fig. 2-6 Scheme of electronic potential in a UPS experiment of a Solid.

reconstruction, and anisotropy of bonding that could give rise to new electronic states, called *surface state.* Owing to lower energy photons in the ultraviolet range and the short mean free path in condensed matter, e.g. [He I ≈ 21.2 eV](585Å), the photoemission becomes much more surface-sensitive.

Fig. 2-6 illustrates the various electronic potentials involved in a UPS experiment of a solid. As the binding energy of an electron in a solid is refereed to E_F, the excited electron kinetic energy upon absorption of a photon above the sample is

$$E_k^{UP} = h\nu - E_b - e\phi \tag{2-3}$$

where E_b is the binding energy of an electron with respect to the Fermi level E_F, thus, the E_b can be determined.

Within the last decade, photoemission from adsorbed layers has proven to be a powerful tool for the study of electronic properties of adsorption systems especially in gas adsorption system. For the metallic thin film system, the energies of adsorbate-induced photoemission peaks become much more important quantities deduced from UPS at the adsorbed layers. However, this bonding shift induced by adsorption of surface atoms should be larger due to the humorous change of orbital energies of chemisorbed particles than for those of physisorbed particles.

2-1-4 Surface Magneto-Optic Kerr Effect (*SMOKE*)

Magneto-optical (MO) effects in magnetic materials can serve as very sensitive probes of the magnetic order. The discovery of the MO effect in 1876 John Kerr observed the rotation of the polarization plane of linearly polarized light upon reflection from the surface of a magnetic piece of iron.[14] Thus, the dependence of the polarization state of light reflected from ferromagnetic surfaces on the magnetization state of the condensed matter, called magneto-optical Kerr effect (MOKE), has been used for many years to observe magnetic domains at bulk magnetic surfaces. The microscopic origin of the MO effects comes from the spin-orbital interaction. The electric and magnetic fields of the incident light affect the orbital motion of the electron, which in turn is coupled via their spins to the magnetization. After Bader et al. noted its easy use to take hysteresis loops from ultrathin films, the effect, called now the surface magneto-optical Kerr effect (SMOKE),[15] has found wide application in ultrathin film magnetism, down to the monolayer. The beauty of SMOKE lies in its simplicity and can help to democratize the field of surface magnetism. Since the rotation of the major axis of the ellipse θ_k and its eccentricity ε_k are proportional to the magnetization M of the material, it is very suitable for probing the surface magnetic microstructure. For most transition metal (TM) compounds, θ_k and ε_k are very small quantities, which are usually smaller than 1° at room temperature.

Three typical types of geometries of the Kerr effect are schematic in the following figures: (a) the polar MOKE, (b) the longitudinal MOKE, and (c) the transversal MOKE.

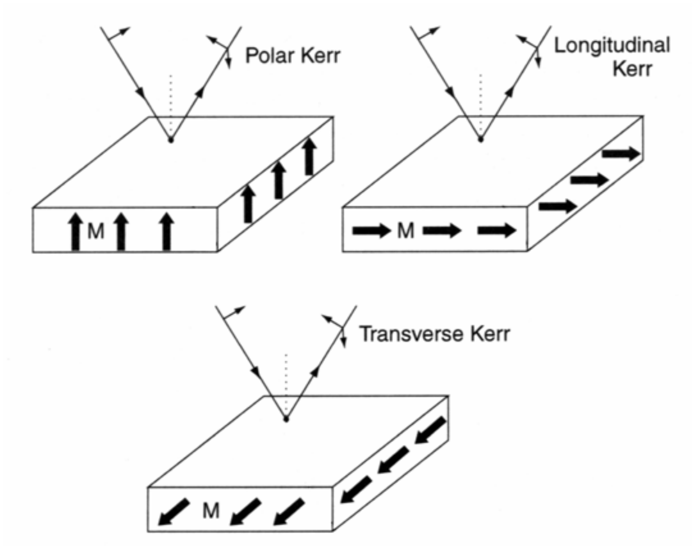

Fig. 2-7 Typical geometries for the magneto-optical Kerr effects. The direction and relative orientations of the magnetization **M** and the polarization of the incident light utilized are illustrated schematically. The incident light is shown plane polarized while the reflected light is in general elliptically polarized.

Experimental L-MOKE studies are less frequent than P-MOKE studies because L-MOKE is measured only at oblique incidence.

SMOKE has emerged as a premier surface magnetism technique of choice found in many laboratories worldwide. Since its ability can generate the hysteresis loop in magnetism. An experimental set-up for measuring the Kerr rotation θ_k in a rather direct way is shown in Fig. 2-8. The incident beam is linearly polarized by a polarizer of fixed position. Then the polarization ellipse of the reflection beam passes through the azimuthal direction polarizer. The vertical-polarized component is proportional to magnetization. The maximum of the photo intensity is referred to the spin up magnetization and the minimum is the spin down magnetization. The Kerr effect implies a rotation of the plane of polarization of linearly polarized light propagating in a magnetic or magnetized medium in a magnetic field. A linearly polarized light has its polarization rotated and it becomes elliptical upon reflection from a magnetized surface. The reflected light is passed through a polarizer that is almost crossed with the polarization of the incident light. When the applied magnetic field is swept through a hysteresis loop, the rotation changes and hence the intensity of the reflected

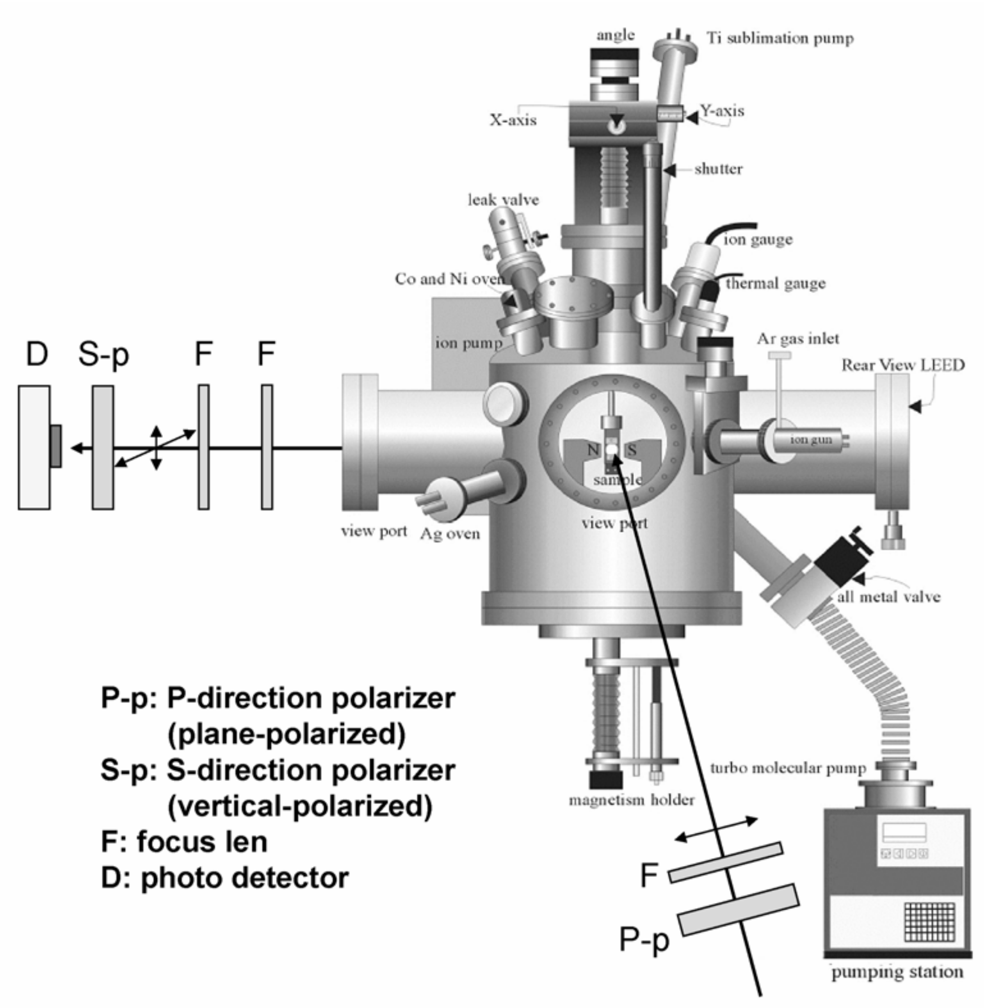

Fig. 2-8 Schematic of SMOKE system

light that passes through the polarizer changes. The rotation is clockwise or counterclockwise depending on if the magnetization of the target sample is spin-up or down.

To provide a quantitative analysis, the Kerr intensity, measured by the photodiode after the laser light passed through an analyzing polarizer that is set at an angle φ from extinction, can be interpreted as

$$I = \left|E_p \sin\varphi + E_s \cos\varphi\right|^2 \approx \left|E_p\varphi + E_s\right|^2 \tag{2-4}$$

where E_p and E_s are denoted as the p- and s- component of electric field, Since $E_s / E_p = \theta_k + i\varepsilon_k$ gives the Kerr rotation θ_k and Kerr ellipticity ε_k, thus Eq. (2-4) becomes

$$I = \left|E_p\right|^2 \left|\varphi + \theta_k + i\varepsilon_k\right|^2 \approx \left|E_p\right|^2 \left(\varphi^2 + 2\varphi\theta_k\right) = I_0\left(1 + \frac{2\theta_k}{\varphi}\right) \tag{2-5}$$

with $I_0 = \left|E_p\right|^2 \varphi^2$ as the intensity at zero Kerr rotation. In other words, the Kerr rotation θ_k can be obtained as half the change of the Kerr intensity in analyzer direction upon magnetization reversal. Thus, the Kerr rotation becomes

$$\theta_k = \frac{\varphi}{4}\frac{\Delta I}{I_0}$$

Using this relation the SMOKE can be used to trace out the magnetic hysteresis loops. More detail description was found in the literatures.[16-18]

2-2 Sample preparation

All experiments were performed *in-situ* in a stainless ultrahigh vacuum (UHV) chamber. The working background pressure maintained about 5×10^{-10} Torr and did not exceed 2×10^{-9} Torr during the deposition. The chamber shown in Fig. 2-9 was equipped with several facilities for the preparation and analysis of thin films and

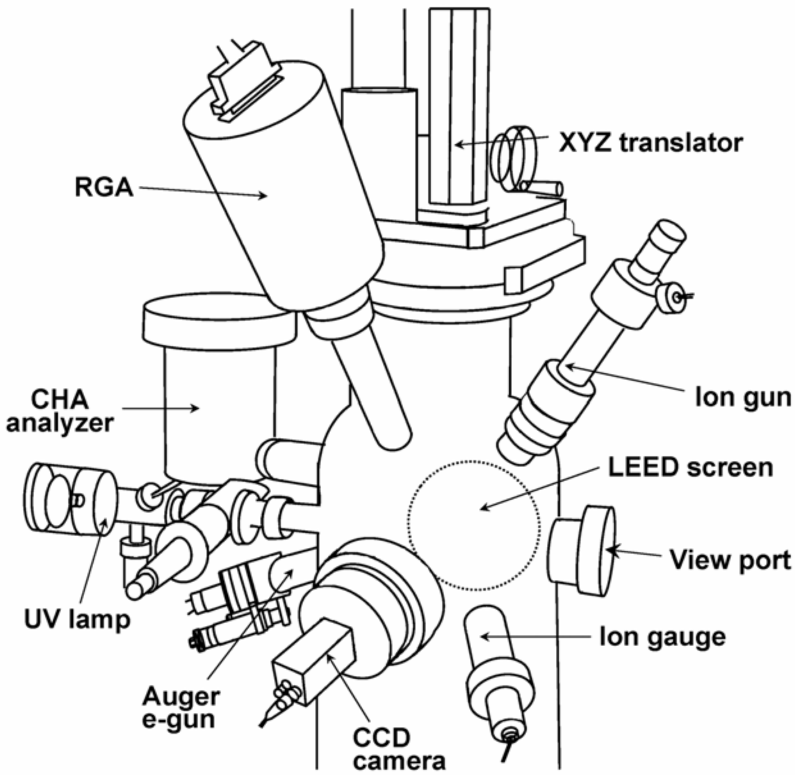

Fig. 2-9 Schematic the UHV system for determining surface structure

surfaces. The surface structure was obtained by four-grid video LEED. The LEED equipped with a computer-controlled video image processor and designed for beam intensity measurements. Besides, a home-made detectable analog-type video screen and a digital camera mounted outside the chamber are used for capture the pattern of

LEED image and monitored the intensity of the diffracted spots of LEED. Also, the chemical compositions of the surface were measured by AES. A UPS with photon energy of He I radiated at the 21.2 eV spectral line. The emitted electrons in the AES and the photoelectrons in the UPS were detected near the sample surface normal. The electron energy analyzer for AES and UPS by different mode was the CLAM-2 cylindrical hemispherical analyzer (CHA) made by VG MICROTECH.

The substrate was one-side polished Pt crystal within 0.5º of the (111)-orientation. The substrate surface of Pt(111) was well prepared by a standard cleaning cycle. The sputtering with energetic ions is an indispensable tool in the cleaning process.[19] Ar^+ source by VG EX03 ion gun system and high-temperature annealing were repeated many times until all residual contamination on the surface, e.g. carbon and oxygen, were below the detectable limit (<1%) of the AES and until the (1×1) sharp threefold low-energy electron diffraction pattern was observed. The bombardment energy and the ion current used in the cleaning process were 2 keV and about 2 ~ 4 μA. The annealing temperature reached 950-1000 K and lasted for an hour, and then cooled slowly (<0.3°C/s) to room temperature for growing samples. Except for the apparatuses used in surface analysis as previously mentioned, turbo molecular pumping system and ion pump were essential for maintaining UHV environment as well.

All samples were *in-situ* fabricated by molecular beam epitaxy (MBE). In this process beams of atoms or molecules in an ultra-high vacuum environment are incident upon a heated crystal that has previously been processed to produce a nearly atomically clean surface.[20] Ni atoms were evaporated from a home-made coil (1 or 0.5mm in diameter) which locked on the feed through with high purity (99.995%) to a well prepared Pt(111)-(1×1) surface. A *k*-type thermocouple was in contact on the Pt(111) substrate. The substrate temperature was kept at 300 ± 3 K during the process of growing Ni thin films. The chamber pressure did not exceed 4×10^{-9} Torr during Ni deposition. Throughout the experiments, the deposition rate of Ni films was carefully controlled by AES calibration to be about one monolayer (ML) per 400 seconds (0.3 Å per minute). Ni LVV (848 eV) and Pt NNV (237 eV) Auger signals were chosen to examine the coverage of Ni thin films. The source of Ag with 99.999% high purity was evaporated from the alumina crucible wound around the home-made heated 1.0 mm tungsten wire. The deposition rates of Ag were calibrated by peak-to-peak intensities from Auger signal of Ag 351 eV versus deposition time (AS-t plot). The deposition rates of Ag were estimated about 0.1 ML/min ($\approx$0.24 Å/min). The Co evaporator with 99.997% purity was evaporated as same as the Ni source. The two-coil evaporator with higher deposition rate about 0.2 ML/min ($\approx$0.4 Å/min) was used for growing Co thin films.